PCCP

Accepted Manuscript

ROYAL SOCIETY OF CHEMISTRY

www.rsc.org/pccp

Effects of Electrolyte, Catalyst, and Membrane Composition and Operating Conditions on the Performance of Solar-Driven Electrochemical Reduction of Carbon Dioxide

Meenesh R. Singh[1], *Ezra L. Clark*[1,2] *and Alexis T. Bell*[1,2,*]

1. *Joint Center for Artificial Photosynthesis, Lawrence Berkeley National Laboratory, Berkeley CA 94720*

2. *Department of Chemical & Biomolecular Engineering, University of California, Berkeley CA 94720*

Submitted to

Physical Chemistry Chemical Physics

June 5, 2015

* Corresponding Author. Email: alexbell@berkeley.edu

ABSTRACT

Solar-driven electrochemical cells can be used to convert carbon dioxide, water, and sunlight into transportation fuels or into precursors to such fuels. The voltage efficiency of such devices depends on the i) physical properties of its components (catalysts, electrolyte, and membrane); ii) operating conditions (carbon dioxide flowrate and pressure, current density); and iii) physical dimensions of the cell. The sources of energy loss in a carbon dioxide reduction (CO2R) cell are the anode and cathode overpotentials, the difference in pH between the anode and cathode, the difference in the partial pressure of carbon dioxide between the bulk electrolyte and the cathode, the ohmic loss across the electrolyte and the diffusional resistances across the boundary layers near the electrodes. In this study, we analyze the effects of these losses and propose optimal device configurations for the efficient operation of a CO2R electrochemical cell operating at a current density of 10 mA cm^{-2}. Cell operation at near-neutral bulk pH offers not only lower polarization losses but also better selectivity to CO2R versus hydrogen evolution. Addition of supporting electrolyte to increase its conductivity has a negative impact on cell performance because it reduces the electric field and the solubility of CO_2. Addition of a pH buffer reduces the polarization losses but may affect catalyst selectivity. The carbon dioxide flowrate and partial pressure can have severe effects on the cell efficiency if the carbon dioxide supply rate falls below the consumption rate. The overall potential losses can be reduced by use of an anion, rather than a cation, exchange membrane. We also show that the maximum polarization losses occur for the electrochemical synthesis of CO and that such losses are lower for the synthesis of products requiring a larger number of electrons per molecule, assuming a fixed current density. We also find that the reported electrocatalytic activity of copper below -1 V vs RHE is strongly influenced by excessive polarization of the cathode and, hence, does not represent its true activity at bulk conditions. This article provides useful guidelines for minimizing polarization losses in solar-driven CO2R electrochemical cells and a method for predicting polarization losses and obtaining kinetic overpotentials from measured partial current densities.

1. INTRODUCTION

The solar-driven electrochemical reduction of atmospheric carbon dioxide to fuels using proton derived from the splitting of water offers a potentially sustainable route for the production of carbon-neutral fuels.[1, 2] Achievement of this capability requires a thorough understanding of the processes occurring in the electrochemical cell where water is oxidized to produce proton and the proton is then used to reduce carbon dioxide. Previous studies have shown that the overall efficiency of carbon dioxide reduction (CO2R) is limited by the overpotentials for the catalysts required to promote the two central reactions – the oxygen evolution reaction (OER)[3, 4] and the carbon dioxide reduction reaction (CO2RR)[1, 5] – and by potential losses due to transport of charged and neutral species occurring in the electrolyte.[6, 7] While the effects of catalyst composition on the overpotentials for the OER and the CO2RR have been discussed extensively in a number of reviews and the references cited therein,[5, 8-10] the influence of transport phenomena has been treated to only a limited degree.[11-13] Gupta et al.[11] have discussed the influence of species transport on the electrochemical reduction of CO_2 in an aqueous solution of $KHCO_3$. Their transport model only considered diffusion of inorganic carbon-containing and hydroxyl species through a boundary layer attached to the cathode but did not include the critical contributions from migration, water dissociation kinetics, proton and potassium balance, and charge balance. A more complete transport model for the electrochemical reduction of CO_2 in aqueous $KHCO_3$ has been presented by Delacourt et al.,[12, 13] but their analysis is specific to the production of synthesis gas at current densities up to 150 mA/cm^2, which are much higher than those envisioned for a photoelectrochemical cell (~10 mA/cm^2). Therefore, there remain many open questions relevant to solar-driven CO2R that need to be addressed. These include: i) What is the optimal pH range for CO2R? ii) Does addition of supporting electrolyte or buffer affect polarization losses? iii) What is the minimum mass-transfer coefficient of CO_2 required to support a current density of 10 mA cm^{-2}? iv) How much mixing is required to support a current density of 10 mA cm^{-2}? v) Does catalyst selectivity affect the polarization losses? vi) What type of ion selective membrane is best suited for CO2R? and vii) How are electrocatalytic measurements affected by polarization of the electrodes? The present study addresses each of these questions with the aim of identifying optimal operating conditions for a planar electrochemical CO2R cell.

The rest of this article is organized as follows. The governing equations, the boundary conditions and the physical parameters used to model a CO2R electrochemical cell are described in Section 2. The effect of pH, current density, conductivity, buffer capacity, boundary layer, CO_2 feed, catalyst selectivity, and membrane on the polarization losses are shown and discussed in Section 3. The concluding remarks are followed by the recommendations for cell design, operating conditions, membrane, and electrolyte selection in Section 5.

2. THEORY

Figure 1 shows a schematic of a one-dimensional photo/electrochemical cell for carbon dioxide reduction. The cell has a well-mixed anolyte and catholyte regions to which carbon dioxide is constantly supplied at fixed partial pressure and flow rate. The anolyte and catholyte are separated by an ion-exchange membrane. The species in the CO_2 equilibrated electrolyte are dissolved CO_2, bicarbonate anions (HCO_3^-), carbonate anions (CO_3^{2-}), protons (H^+), hydroxide anions (OH^-), and potassium cations (K^+). Other cations and anions may also be present, if a supporting electrolyte is added.

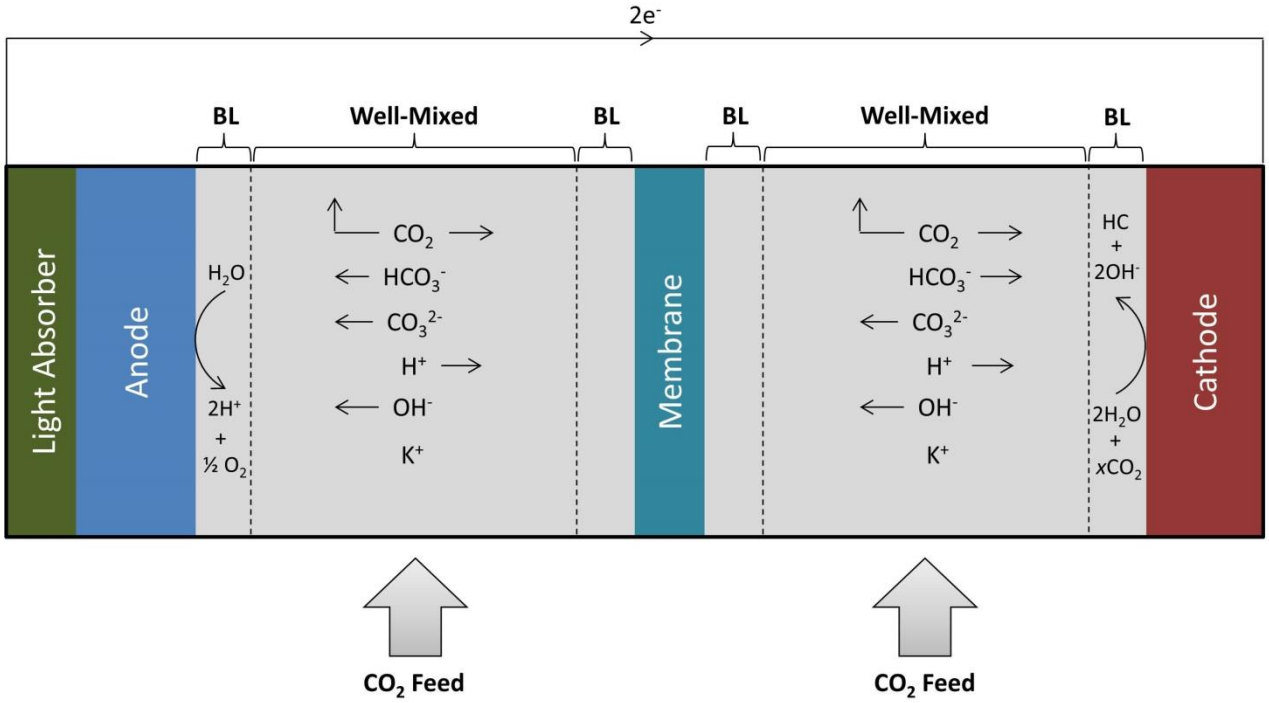

Figure 1: Schematic diagram of a one-dimensional photo/electrochemical carbon dioxide reduction cell. Carbon dioxide is fed into a well-mixed region where the directions of steady-state transport of species are shown by the straight arrows. The holes produced by the light absorber oxidize water at the anode and the corresponding electrons reduce carbon dioxide to products (HC) at the cathode. The reactants and products diffuse and migrate through the boundary layers (BL).

2.1 Polarization Losses

Polarization loss due to transport of species (by migration and diffusion) and concentration gradients can be represented as a sum of i) ohmic loss, ii) diffusion loss, and iii) Nernstian loss. The ohmic loss is due to the resistance of the electrolyte, and the diffusion loss originates from the ionic gradient in the boundary layer near each electrode due to the applied current density. The ohmic and diffusion losses can be combined into the solution loss such that

$$\Delta\phi_{\text{solution}} = \underbrace{\int \frac{i_l}{\kappa} dx}_{\Delta\phi_{\text{ohmic}}} + \underbrace{\sum_i \int \frac{F z_i D_i \nabla c_i}{\kappa} dx}_{\Delta\phi_{\text{diffusion}}} \quad (1)$$

where i_l is the electrolyte current density, κ is the electrolyte conductivity, x is the position, F is Faraday's constant, z_i is the charge number, D_i is the diffusion coefficient, and c_i is the concentration of the i^{th} species. The ionic gradients shift the concentrations of reacting species next to the electrode surfaces (e.g., protons, hydroxide anion, and dissolved carbon dioxide) away from those present in the bulk. This causes an increase in the equilibrium potential of the oxygen evolution reaction (OER) and the carbon dioxide reduction reaction (CO2RR), which are referred to collectively as the Nernstian loss. The sum of losses due to differences in pH at the two electrodes, and differences in concentration of carbon dioxide at the cathode and in the bulk electrolyte is given by

$$\Delta\phi_{\text{Nernstian}} = \underbrace{\frac{2.303RT}{F}\left(\text{pH}_{\text{cathode}} - \text{pH}_{\text{bulk}}\right)}_{\Delta\phi_{\text{cathode pH}}} + \underbrace{\frac{2.303RT}{F}\left(\text{pH}_{\text{bulk}} - \text{pH}_{\text{anode}}\right)}_{\Delta\phi_{\text{anode pH}}} + \underbrace{\frac{RT}{nF}\ln\left(\frac{p_{\text{CO}_2,\,\text{bulk}}}{p_{\text{CO}_2,\,\text{cathode}}}\right)}_{\Delta\phi_{\text{cathode CO}_2}} \quad (2)$$

where R is the gas constant, T is the temperature, n is the moles of electron transferred per mole of CO_2, and p_{CO_2} is the partial pressure of carbon dioxide. The Nernstian loss due to pH change at the cathode will be referred to as the *cathode pH loss*, that due to the pH change at the anode will be referred to as the *anode pH loss*, and that due to change in the CO_2 concentration at the cathode will be referred to as the *CO_2 loss*. The losses given by Equation (1) and (2) are due to transport of species in the electrolyte, which, in turn, depend on the applied current density, electrolyte composition, electrolyte hydrodynamics , carbon dioxide feed concentration and rate, membrane composition, and catalyst selectivity. The kinetic overpotentials for the OER and CO2RR also contribute to the total losses in the electrochemical cell.

2.2 Acid-Base Equilibria

The amount of carbon dioxide dissolved in the electrolyte depends on the pressure, temperature, and salinity[†] of the electrolyte. The equilibrium of CO_2 between gas and liquid phase,

$$\text{CO}_{2(\text{g})} \rightleftharpoons \text{CO}_{2(\text{aq})} \quad (3)$$

is given by the Henry's constant $\left(K_0\right)$, such that

[†] Salinity is defined as the total amount of salt (in grams) dissolved in 1 kg of solution. The unit of salinity is given in parts per thousand (‰).

$$K_0 = \frac{c_{CO_2}}{f_{CO_2}} \tag{4}$$

where c_{CO_2} is the concentration of dissolved carbon dioxide, and f_{CO_2} is the fugacity of carbon dioxide in gas phase. The dependence of the Henry's constant on the temperature (T, in Kelvin) and salinity (S, in parts per thousand) at ambient pressure is given as[14]

$$\begin{aligned} \ln(K_0) = {} & 93.4517\left(\frac{100}{T}\right) - 60.2409 + 23.3585\ln\left(\frac{T}{100}\right) \\ & + S\left(0.023517 - 0.023656\left(\frac{T}{100}\right) + 0.0047036\left(\frac{T}{100}\right)^2\right) \end{aligned} \tag{5}$$

This empirical relationship shows that the solubility of carbon dioxide decreases with increasing total salt concentration, a phenomenon known as the "salting-out" effect.

The dissolved CO_2 can also be hydrated to form carbonic acid, but its concentration is only about 1/1000 of the concentration of dissolved CO_2.[15] Therefore, we do not distinguish between the hydrated and dissolved CO_2, and consider them as a single species. The dissolved CO_2 dissociates to produce bicarbonate and carbonate ions when pH is greater than 5. The corresponding pair of reactions is given as

$$CO_{2(aq)} + H_2O \underset{k_{-1}}{\overset{k_{+1}}{\rightleftharpoons}} H^+ + HCO_3^-, \quad pK_1 = 6.37 \tag{6}$$

$$HCO_3^- \underset{k_{-2}}{\overset{k_{+2}}{\rightleftharpoons}} H^+ + CO_3^{2-}, \quad pK_2 = 10.25 \tag{7}$$

The values of forward rate constants of reactions (6) and (7) are $k_{+1} = 3.71\times10^{-2}\ s^{-1}$ and $k_{+2} = 59.44\ s^{-1}$, respectively.[16] The reverse rate constants can be obtained from pK_1 and pK_2 for reactions (6) and (7), respectively. The dependence of the equilibrium constants on temperature and salinity can be found elsewhere.[14] We also include the bulk ionization of water,

$$H_2O \underset{k_{-w}}{\overset{k_{+w}}{\rightleftharpoons}} H^+ + OH^- \tag{8}$$

The value of the forward rate constant of water ionization is $k_{+w} = 2.4\times10^{-5}\ mol\,L^{-1}\,s^{-1}$ and the equilibrium constant is $K_w = 1\times10^{-14}\ mol^2\,L^{-2}$.[17]

2.3 Transport of Species in the Electrolyte and Membrane

The transport of species in the electrolyte and membrane must satisfy mass conservation, such that

$$\frac{\partial c_i}{\partial t} + \frac{\partial N_i}{\partial x} = R_i \tag{9}$$

where N_i is the molar flux, and R_i is the volumetric rate of formation of species i (CO_2, HCO_3^-, CO_3^{2-}, H^+, OH^-, K^+, and Cl^-). The rate of production of species i, R_i, can be determined from reactions (6), (7), and (8). The molar flux of species in dilute electrolyte can be written as a sum of fluxes due to diffusion and migration.

$$N_i = -D_i \frac{\partial c_i}{\partial x} - z_i u_i F c_i \frac{\partial \phi_l}{\partial x} \tag{10}$$

where u_i is the mobility of ion given by the Nernst-Einstein relationship, and ϕ_l is the electrolyte potential. The diffusion coefficients of species in the dilute electrolyte are given in Table 1. We neglect the variation of diffusion coefficients with the electrolyte concentration, as the variation is marginal for dilute electrolytes (< 10 mol%).[18]

Table 1: Diffusion coefficients of species in water at infinite dilution at 25℃ [19, 20]

Species	**Diffusion Coefficient (10^{-9} m^2 s^{-1})**	**Mobility (10^{-7} m^2 V^{-1} s^{-1})**
CO_2	1.91	-
HCO_3^-	1.185	0.462
CO_3^{2-}	0.923	0.359
H^+	9.311	3.626
OH^-	5.273	2.054
K^+	1.957	0.762
Cl^-	2.032	0.791

The electrolyte current density i_l can be obtained from the total ionic flux,

$$i_l = F \sum_i z_i N_i \tag{11}$$

and the assumption of electro-neutrality,

$$\sum_i z_i c_i = 0 \tag{12}$$

The same set of equations [(9) - (12)] were used to model the boundary layer region, the well-mixed region, and the membrane. Expressions for the rate of CO_2 transfer to or from the electrolyte, and diffusion coefficients for transport of ions through the membrane are discussed in the next three subsections.

Well-Mixed Electrolyte

The well-mixed region of the electrolyte, as shown in Figure 1, was assumed to have no diffusional resistance and therefore charged species are transported only by migration. The net rate formation of HCO_3^-, CO_3^{2-}, H^+, OH^- were set to zero in the bulk because reactions 6, 7, and 8 were assumed to be at equilibrium. Therefore, only the rate of CO_2 transfer from gas phase to liquid phase was non-zero. A constant feed of CO_2 in the well-mixed region was included as an additional generation term on the right side of equation (9), given as

$$R_{\mathrm{CO_2,\,feed}} = k_l a\, \delta\, K_0\, f_{\mathrm{CO_2}} \tag{13}$$

where $k_l a$ is the volumetric mass-transfer coefficient (unit: s^{-1}) on the liquid side of gas-liquid interface, and δ is the fraction of inlet CO_2 transferred from the gas phase to the liquid phase. In the present scenario, the volumetric mass-transfer coefficient is equivalent to the inverse of the residence time of gas bubbles. The typical ranges for $k_l a$ and δ are $10^{-2} - 10^{0}$ s^{-1} (refs. 21, 22) and < 0.01 (ref. 2), respectively. For the present study we have chosen $k_l a\,\delta = 0.33\ s^{-1}$ to ensure that the bulk electrolyte is always saturated with CO_2 and the current density is not limited by the mass-transfer of CO_2 in the bulk. The effect of the mass-transfer coefficient on the polarization losses will be discussed in section 3.7. We have also fixed the boundary layer thickness to 100 μm in all simulations except for the results shown in section 3.6.

Evolution of CO_2 at Anode

As will be shown, at high current densities the boundary-layer region near the anode can become acidic. When this happens, the concentration of CO_2 in the bulk electrolyte will be supersaturated above the saturation level predicted for the anode boundary layer and consequently bubble-out of the electrolyte in this region. Therefore, it is essential to continuously feed CO_2 to the anolyte to avoid depletion of CO_2 and hence the bicarbonate buffer. Consequently, a higher pH changes at the anode can be observed in the absence of CO_2 feed in the anolyte.

Wilt has shown that the homogenous nucleation of CO_2 in carbonated water requires supersaturation three orders of magnitude higher than the saturation level at room temperature and, therefore, concludes that heterogeneous nucleation is the principal mechanism for CO_2 evolution from aqueous solution[23] Moreover, he proposes that the rate of nucleation on a rough surface with conical cavities is second order in the supersaturation for low levels of supersaturation ($S < 2$).[23] Therefore, we represent the evolution CO_2 as a boundary condition at the anode. The rate of CO_2 evolution per unit of anode area is given by

$$\begin{aligned} N_{\mathrm{CO_2}} &= -N_0 \nu_0 \mathrm{V_m^{-1}} S^2 \quad && S > 1 \\ &= 0 && S \le 1 \end{aligned} \tag{14}$$

where N_0 is the number of CO_2 gas bubbles nucleated per unit area unit time, v_0 is the average volume of CO_2 gas bubble, V_m is the molar volume of CO_2 gas which is $41.85\ m^3mol^{-1}$, and $S \equiv c_{CO_2} / K_0 f_{CO_2}$ is the supersaturation. The values of $N_0 = 1\times10^{25}\ m^{-2}s^{-1}$ and $v_0 = 5.24\times10^{-19}\ m^3$ are chosen so that the nucleation rate matches the values reported by Wilt[23].

Membrane

The cation exchange membrane (CEM) was modeled as an electrolyte with a background negative charge of 1 M and modified diffusion coefficients. The diffusion coefficients of cations were reduced by a factor of 10 (ref. 24) and that of anions were reduced by a factor of 100 (refs. 25, 26) relative to those for cations and anions, respectively, in the liquid electrolyte. Similarly, an anion exchange membrane (AEM) was assumed to have a fixed background positive charge of 1 M, and anion and cations diffusion coefficients reduced by a factor of 10 (ref. 27) and by a factor of 100 (assumed), respectively, relative to those for transport in the electrolyte.

2.4 Surface Reactions at Anode and Cathode

Charge-transfer kinetics at the anode and cathode were modeled using Butler-Volmer kinetics, such that

$$i_s = i_l = i_R = i_0\left[e^{\frac{\alpha_a F\left(\phi_s-\phi_l-E^0\right)}{RT}} - e^{-\frac{\alpha_c F\left(\phi_s-\phi_l-E^0\right)}{RT}}\right] \tag{15}$$

where i_s is the electrode current density, i_R is the reaction current density, E^0 is the equilibrium potential of the half-reaction of interest (which depends upon the pH and on the partial pressure of gases), ϕ_s is the electrode potential, i_0 is the exchange-current density, and α_a and α_c are the anodic and cathodic transfer coefficients, respectively. The kinetic overpotential of a catalyst is given by $\eta = \phi_s - \phi_l - E^0 + \Delta\phi_{\text{Nernstian}}$.

The half-cell reaction at the anode is the oxidation of water, which creates acidic conditions near the electrode.

$$H_2O \rightarrow \frac{1}{2}O_2 + 2H^+ + 2e^-, \quad E^0 = 1.229\,V \tag{16}$$

For the work reported here, the kinetics of water oxidation on IrO_2 was used for the anode due to its stability under acidic conditions and its low overpotential for oxygen evolution.[4] The kinetic parameters are given in Table 2.

Table 2: Butler-Volmer parameters for the oxygen evolution reaction (OER), and carbon monoxide evolution reaction (CER).

Reaction	**Catalyst**	i_0 **(A m^{-2})**	α_a	α_c
OER[4]	IrO_2	1.4×10^{-3}	1	0.1
CER[28]	Ag	1.5×10^{-3}	0	0.285

The cathode reactions involve the reduction of carbon dioxide and water. As shown below, these reactions occur under alkaline conditions and, hence, can be written as:.

$$\begin{aligned}
2H_2O + 2e^- &\rightarrow H_2 + 2OH^- && E^0 = 0\,V \\
CO_2 + H_2O + 2e^- &\rightarrow CO + 2OH^- && E^0 = -0.10\,V \\
CO_2 + 2H_2O + 2e^- &\rightarrow HCOOH + 2OH^- && E^0 = -0.02\,V \\
CO_2 + 5H_2O + 6e^- &\rightarrow CH_3OH + 6OH^- && E^0 = +0.03\,V \\
CO_2 + 6H_2O + 8e^- &\rightarrow CH_4 + 8OH^- && E^0 = +0.17\,V \\
2CO_2 + 8H_2O + 12e^- &\rightarrow C_2H_4 + 12OH^- && E^0 = +0.08\,V
\end{aligned} \tag{17}$$

These reactions produce one hydroxide ion per electron transferred. However, the stoichiometric amount of CO_2 consumed per electron transferred varies for each CO2R product. Therefore, maximum polarization in the electrochemical cell will be observed for the carbon monoxide evolution reaction (CER) which has highest stoichiometric ratio (0.5) for CO_2.

2.5 Electrode Current Density

The current density at a metal electrode is given by Ohm's law:

$$i_s = -\kappa_s \frac{\partial \phi_s}{\partial x} \tag{18}$$

where κ_s is the conductivity of the electrode.

To maintain electroneutrality, the divergence of current density in the solid and the liquid must be zero:

$$\frac{\partial i_l}{\partial x} = 0, \quad \frac{\partial i_s}{\partial x} = 0 \tag{19}$$

The potential in the electrochemical cell was calculated relative to zero potential at cathode, and the anode was assumed to have a fixed current density which can be supplied by a photoactive material.

Equations (3) - (19) were solved using COMSOL Multiphysics 4.3b, and the polarization losses are obtained by post-processing the simulation results according to equations (1) and (2).

2.6 Prediction of Polarization Losses on Silver and Copper Cathodes

The polarization losses were determined for a number of scenarios. In Sections 3.2-3-8 these calculations are reported for a cell containing an Ag cathode and an IrO_2 anode, assuming that Faradaic efficiencies for O_2 and CO formation are 100% in both cases. Two different scenarios are compared in Section 3.9. The first two are for a cell containing an IrO_2 anode and an Ag cathode in which CO is formed with a Faradaic efficiency of 100% or CO and H_2 are formed over a Ag cathode with the Faradaic efficiencies reported by Hatsukade et al.[28] The kinetic parameters for cathodic reactions are also given in Table 2.

The partial current densities of CO2RR products formed at a Cu cathode and the corresponding Faradaic efficiencies were used to predict polarization losses in the electrochemical cell of Kuhl et al.[2] and are reported in Section 3.10. We use the same set of equations to predict polarization losses except that the boundary condition (15) for cathode was replaced by the measured partial current densities. Since the polarization of the cathode is insensitive to the anode catalyst, we have used the kinetics for an IrO_2 anode instead of the Pt anode as used by Kuhl et al. The electrochemical cell has 8 ml of 0.1 M $KHCO_3$ on each side of a Selemion AMV, continuously sparged with 20 cm^3 min^{-1} of CO_2, and an electrode area of 4.5 cm^2. The distance between the anode and cathode is ~3.56 cm. The measured cyclic voltammogram indicates the limiting current density of ~22 mA cm^{-2}, which corresponds to a mean boundary layer thickness of 40 μm. The above information was used to predict kinetic overpotentials of CO2RR products on the Cu cathode for the data reported by Kuhl et al.[2]

3. RESULTS AND DISCUSSION

3.1 Speciation in the Carbonated Electrolyte

The distribution of species (CO_2, HCO_3^-, CO_3^{2-}, OH^-, H^+, and K^+) in a CO_2-saturated electrolyte is described by three reactions (Eqs. (6), (7), and (8)), and is constrained by the requirement that the solution be electroneutral (Eq. (12)). Therefore this system has two degrees of freedom. Setting the concentrations of CO_2 and H^+ (or the pH) in the electrolyte automatically fixes the equilibrium concentrations of the remaining species. Alternatively, one can independently set the conductivity and pH of the electrolyte. Figure 2 shows the concentration of dissolved carbon-containing species in the potassium bicarbonate/carbonate electrolyte as a function of pH for a temperature of 25℃ and a total pressure of 1 atm.

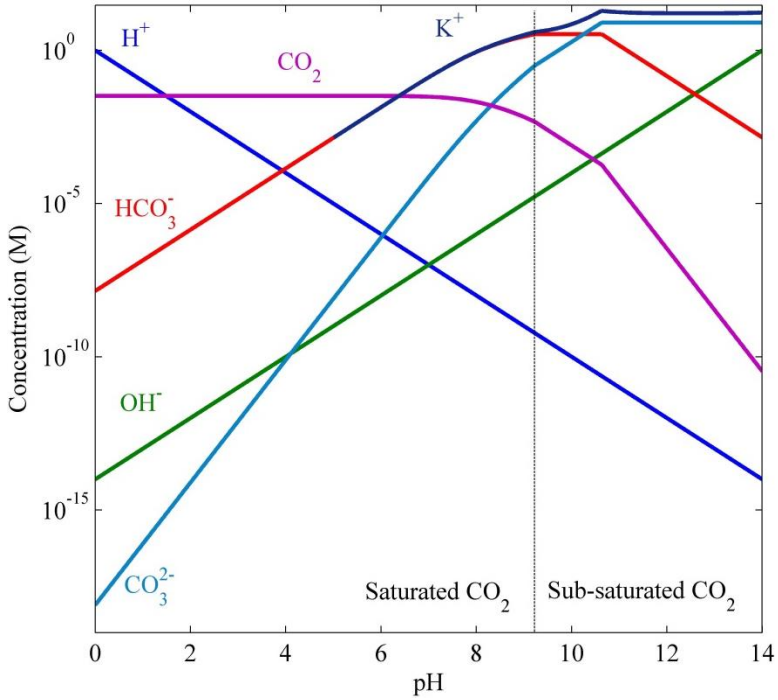

Figure 2: Concentration of carbon dioxide, hydrogen, hydroxyl, bicarbonate, carbonate, and potassium ions as a function of bulk pH of the potassium bicarbonate/carbonate electrolyte at 25℃ and a total pressure of 1 atm. For pH < 9.22, the partial pressure of CO_2 is 1 atm. For pH = 9.22, the solubility limit of $KHCO_3$ is reached, and for pH = 10.6, the solubility limit of K_2CO_3 is reached. Consequently, the partial pressure of CO_2, and hence the concentration of dissolved CO_2 must be reduced to avoid precipitation of $KHCO_3$ and K_2CO_3 for pH > 9.22.

The dominant carbon-containing species in the electrolyte for pH < 5 is molecular carbon dioxide which has a solubility of ~ 33 mM at 25℃ and 1 atm of CO_2. The additional species

present for pH < 5 are H^+, the anion of the acid (e.g., Cl^-), which is not shown, and OH^-, HCO_3^- and CO_3^{2-}, which are present in only very low concentrations. With increasing pH the concentrations of HCO_3^- and CO_3^{2-} increase, and hence the required concentration of K^+, whereas the concentration of the anion of the acid decreases so as to maintain charge balance. The majority species in the pH range from 5 to 8 are K^+, CO_3^{2-}, and dissolved CO_2. The concentration of dissolved CO_2 decreases as a consequence of increasing concentrations of potassium bicarbonate and potassium carbonate in this pH range, a consequence of the "salting out" effect. The concentration of $KHCO_3$ reaches its solubility limit at pH 9.22. Therefore, to prevent solid formation the concentration of dissolved CO_2 must decrease below the saturation level for pH > 9.22. Above a pH of 10.6 precipitation of K_2CO_3 can occur, and consequently the concentration of dissolved CO_2 must decrease further.

3.2 Effect of Electrolyte pH

The limiting reactant in the electrochemical CO2R can be either carbon dioxide or protons. The rate of consumption of the reactants is linearly dependent on the current density. Therefore, the reactant concentrations at the cathode decrease with increasing current density and can eventually reduce to a negligible value. The current density under such situation is limited by the mass-transfer of reacting species to the cathode, and is known as the *limiting current density*. The limiting current density is the maximum current density at which the electrochemical reaction can occur. Figure 3a shows the variation in the limiting current density as a function of pH of the electrolytes for a fixed conductivity of 4 S m^{-1} in a membrane-free cell. The concentrations of species in the electrolytes of different pH follow a trend similar to that shown in Figure 2. The fixed electrolyte conductivity of 4 S m^{-1} imposes a limit on the maximum allowable ionicity of the electrolyte, which, in turn, determines the pH range ($1 \leq pH \leq 7.4$) over which the electrolyte can be saturated with CO_2. Therefore, to prepare electrolytes with pH > 7.4 and a conductivity of 4 S m^{-1}, the partial pressure of CO_2 must be reduced below 1 atm. The plot shows three marked regions – the first region ($1 \leq pH < 2$) corresponds to strongly acidic electrolyte, the second region ($2 \leq pH < 4$) corresponds to mildly acidic electrolyte, and the third region corresponds to $pH \geq 4$. The strongly acidic region has a higher concentration of protons than carbon dioxide, which makes the CO_2 reduction current density limited by mass transport of carbon dioxide to the cathode. The limiting current density in the strongly acidic regime decreases with increasing pH. The mildly acidic regime is limited by the transport of protons because the concentration of protons is lower than the concentration of carbon dioxide.

Interestingly, the proton-limited current density exhibits minimum at around pH = 3. Thereafter, the limiting current density increases steadily up to ~ pH = 8 and then decreases down to a negligible level past pH = 11. Although the region past pH 4 has a much lower concentration of protons, the current is limited by the mass transfer of carbon dioxide to the cathode. This is due to facilitated transport of protons through bicarbonate ions, which acts as a buffer and can readily dissociate to give protons. Figure 3a also shows that the CO_2-limited

current density increases with the increase in the concentration of bicarbonate ions up to pH = 8. The decrease in the limiting current density beyond pH = 8 is due to the decrease in the concentration of CO_2 required to maintain a conductivity of 4 S m^{-1} (cf. Figure 2). The limiting current density has maxima around pH = 1 and pH = 8, which also result in lower polarization losses.

The total polarization loss is the sum of solution and Nernstian losses, given as

$$\Delta\phi_{\text{polarization}} = \Delta\phi_{\text{solution}} + \Delta\phi_{\text{Nernstian}} \tag{20}$$

Figure 3b shows the polarization losses for a current density of 10 mA cm^{-2} in a membrane-free cell. The polarization loss increases with the pH in the strongly acidic regime, where the dominant source of the potential loss before reaching the limiting current density is the CO_2 loss. However, the cathode pH loss becomes dominant and takes over the CO_2 losses at around pH = 2. Although the high concentration of protons in strongly acidic electrolytes can help to minimize polarization losses and the pH change at the electrodes, it can affect electrode stability and give rise to an increase in hydrogen evolution over CO_2 reduction.

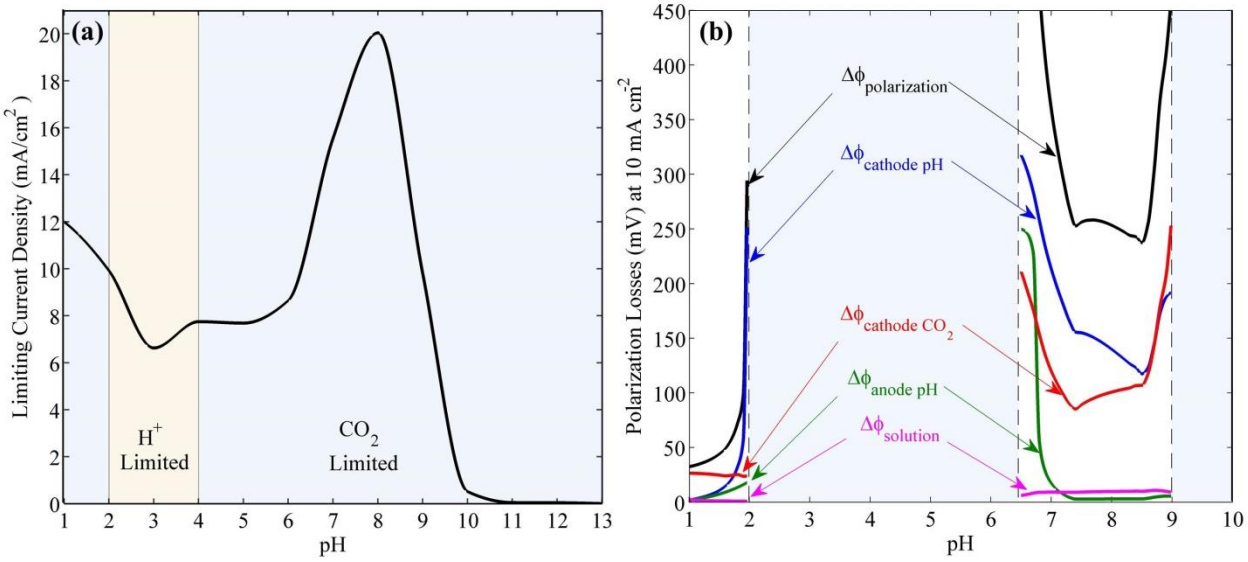

Figure 3: (a) Limiting current density versus pH and (b) Polarization losses at current density of 10 mA cm^{-2} versus pH. Operating conditions: $\kappa = 4$ S m^{-1}, no membrane, boundary layer thickness = 100 µm, and $k_l a\,\delta = 0.33\ s^{-1}$.

The shaded region (- 2 ≤ pH ≤ 6.5, and pH ≥ 9) in Figure 3b corresponds to unbounded polarization losses when the applied current density is higher than the limiting current density. Generally, the polarization losses in the shaded region are higher than those for acidic and near-neutral pH electrolytes. The lower polarization losses in near neutral pH (6.5 < pH < 9) electrolytes is due to the presence of bicarbonate ions. Despite the buffering capacity of bicarbonate ions, the cathode pH loss still dominates in this region. The polarization loss in the

near neutral pH regime shows a minimum of 237 mV at pH 8.5. However, the lowest CO_2 loss is observed at pH 7.4. The solution loss is < 11 mV throughout the pH range. The anode pH loss is also very low except near pH = 2 and 6.5, where it is comparable to the CO_2 loss. Interestingly, the anode pH loss is not as severe as the cathode pH loss. The depletion of CO_2 due to its consumption at the cathode also reduces the concentration of bicarbonate ions (cf. (6)). The decrease in the buffering capacity at the cathode increases the pH near this electrode more rapidly than that near the anode.

3.3 Effect of Current Density

The maximum photocurrent density for CO2RR that can be obtained from an ideal triple-junction light absorber is < 18 mA cm^{-2}.[29] Figure 4a shows the kinetic overpotentials for the CER and OER, and the polarization losses as a function of photocurrent densities from light absorber. These individual losses along with equilibrium potential determine the total voltage requirement of an electrochemical cell, which is given by:

$$\mathrm{V}(i) = E^0_{OER} - E^0_{\mathrm{CO2RR}} + \eta_{\mathrm{OER}}(i) - \eta_{\mathrm{CO2RR}}(i) + \Delta\phi_{\mathrm{solution}}(i) + \Delta\phi_{\mathrm{Nernestian}}(i) \qquad (21)$$

where η_{OER} and η_{CO2RR} are the kinetic overpotentials for the OER and the CO2RR, respectively, and E^0_{OER} and E^0_{CO2RR} are the equilibrium potentials of the OER and CO2R reactions, respectively. Clearly, the largest potential loss is due to the overpotential of the CER for which the onset potential is ~800 mV. The second largest potential loss is due to overpotential of OER. The majority of the polarization loss comes from the increase in the pH and the decrease in the concentration of CO_2 at the cathode. The distribution of polarization losses for a current density of 10 mA cm^{-2} is as follows: cathode pH loss, ~64%, CO_2 loss, ~33%, solution loss, ~2%, and anode pH loss, ~1%. The following pattern of polarization losses is invariant with the current density.

$$\Delta\phi_{\text{cathode pH}} > \Delta\phi_{\text{cathode CO}_2} > \Delta\phi_{\text{solution}} > \Delta\phi_{\text{anode pH}}$$

The value of $\Delta\phi_{\text{cathode pH}}$ and $\Delta\phi_{\text{anode pH}}$ is 59 mV per unit pH change at cathode and anode, respectively. The value of $\Delta\phi_{\text{cathode CO}_2}$ is 59/n mV per order of magnitude change in the concentration of CO_2 at the cathode, where n is the number of electrons consumed in the CO2RR.

Figure 4b shows the variation in the concentrations of carbon-containing species, hydroxide anions, and protons near the cathode with the current density. The surface concentration of carbon dioxide at 10 mA cm^{-2} is 0.66 mM, approximately two orders of magnitude lower than the saturation limit. Also the cathode surface pH at 10 mA cm^{-2} is 9.45, or 1.65 pH units higher than the bulk pH of 7.8 (which corresponds to 1M $KHCO_3$). The corresponding cathode pH and CO_2 losses at 10 mA cm^{-2} are ~96 mV and ~50 mV, respectively.

The polarization losses at the cathode seen in Figure 4a are consistent with the surface concentrations in Figure 4b. The solution loss, $\Delta\phi_{\text{solution}}$, is mostly governed by the conductivity of the electrolyte, whose effect is discussed next.

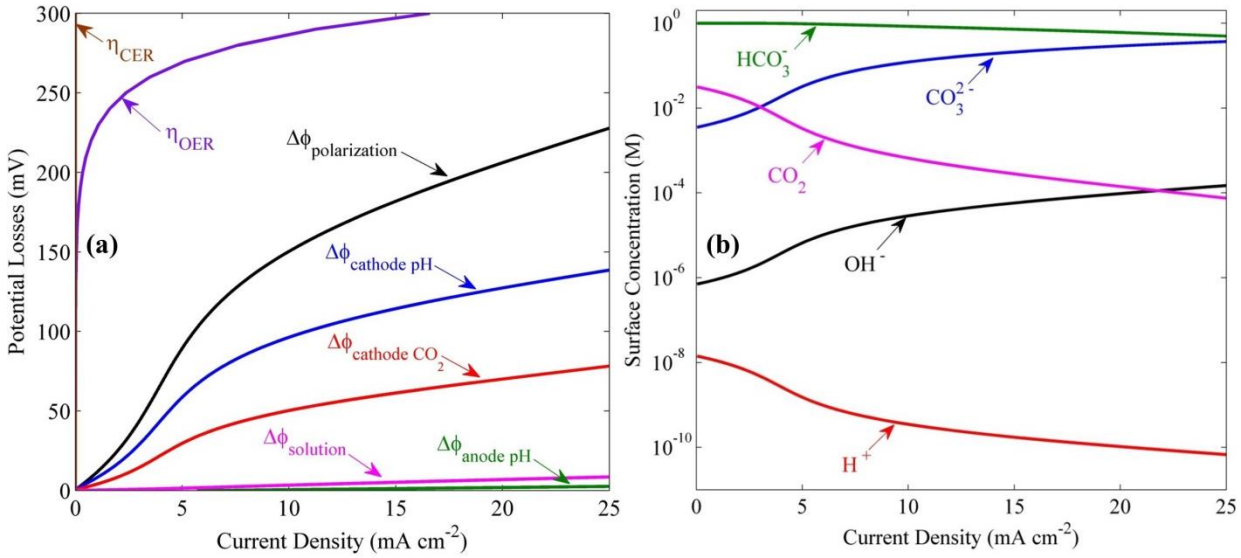

Figure 4: (a) Potential losses and (b) cathode surface concentrations versus current density. Operating conditions: pH 7.8, 1 M $KHCO_3$, no membrane, $p_{CO_2} = 1\,\text{atm}$, boundary layer thickness = 100 μm, and $k_l a\,\delta = 0.33\ \text{s}^{-1}$.

3.4 Effect of Electrolyte Conductivity

Figure 5 shows the effect of adding supporting electrolyte (potassium chloride) on the polarization losses in 1M $KHCO_3$ at 10 mA cm^{-2}. The conductivity of this electrolyte can be increased by adding a supporting electrolyte, such as KCl. For instance, the addition of 3M KCl increases the conductivity and salinity of the electrolyte to 37 S m^{-1} and 300 ‰, respectively. The increase in the salinity/conductivity of electrolyte has two effects – i) reduction of the electric field (see Eq. (1)), and ii) salting-out of CO_2 (see Eq.(5)). The reduction of the electric field decreases the migration of ions, which is followed by an increase in the diffusional flux to support the same current density. The following equation shows how the concentration gradient must increase to balance the drop in potential gradient (or electric field) at a fixed current density.

$$i_l = -\sum_i \underbrace{z_i F D_i \frac{\partial c_i}{\partial x}}_{i_{\text{diffusion}}} + \underbrace{z_i^2 u_i F^2 c_i \frac{\partial \phi_l}{\partial x}}_{i_{\text{migration}}} \qquad (22)$$

The increase in the concentration gradients increases the deviation of pH and CO_2 concentration at the electrodes, which in turn increases the Nernstian losses. Additionally, the lower solubility of CO_2 (~0.7 mM with 3M KCl) in the saline electrolyte causes even more depletion of CO_2 at the cathode. Consequently, the polarization losses except for the solution loss increase monotonically with the conductivity. The solution loss decreases with conductivity according to Equation (1). The net polarization loss increases at the rate of ~3.5 mV S^{-1} m. The individual rates of change of polarization losses with conductivity for i) cathode pH loss is 1.77 mV S^{-1} m, ii) CO_2 loss is 1.59 mV S^{-1} m, iii) anode pH loss is 0.23 mV S^{-1} m, and iv) solution loss is -0.08 mV S^{-1} m.

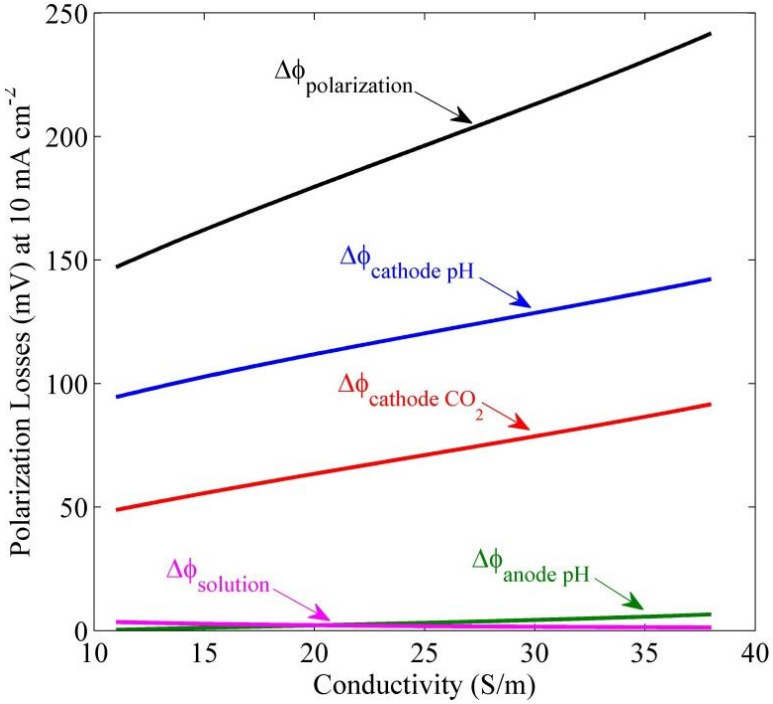

Figure 5: Variation of the polarization losses with the conductivity. Operating conditions: pH 7.8, 1 M $KHCO_3$, no membrane, i_l=10 mA cm^{-2}, p_{CO_2} =1 atm, boundary layer thickness = 100 µm, and $k_l a\delta = 0.33\ s^{-1}$.

3.5 Effect of Buffer

Buffers such as acetate, phosphate, and borate salts dissociate when the cathode pH goes above their pKa values, and hence help to minimize pH changes at the electrodes. Figure 6 shows the effect of buffer concentration on the polarization loss in 1M $KHCO_3$ electrolyte. The buffered electrolyte contains equimolar quantities of conjugated acid (HA) and conjugated base (A^-) species, such that the pKa of buffer is equal to the pH 7.8. The majority of the overall polarization loss, ~97%, is due to polarization of the cathode and can be minimized with the addition of buffer The polarization loss at 10 mA cm^{-2} using buffer concentrations of 0 M, 0.1 M,

0.5 M, and 1 M are 150.3 mV, 104.3 mV, 32.6 mV, and 19.55 mV, respectively. Generally, the polarization losses decrease with increasing buffer concentration because the majority charge carriers in such buffered electrolytes are A^-, CO_3^{2-}, and HCO_3^-. Since the protons and hydroxide anions are minority charge carriers, the pH gradients are very low. The gradient in CO_2 concentration is also decreases with pH gradient. Although the use of pH buffer shows promise for minimizing polarization losses, it can have a negative effect on the CO2RR selectivity due to the reactivity of the conjugate acid towards hydrogen evolution (i.e., $2H_2PO_4^- + 2e^- \rightarrow H_2 + 2HPO_4^{2-}$).[30]

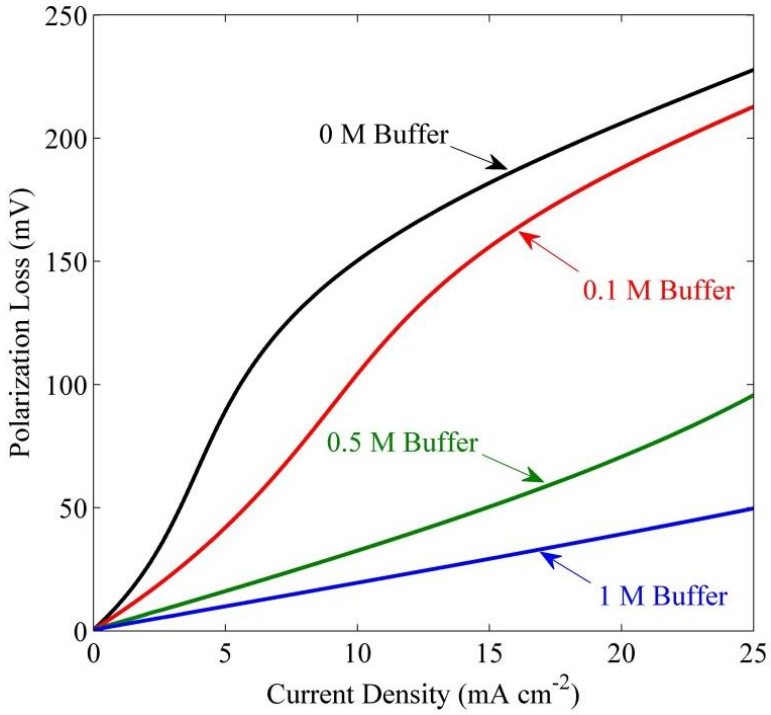

Figure 6: Polarization loss versus current density for 0.1 M, 0.5 M, and 1 M buffered electrolyte. Operating conditions: pH 7.8, 1 M $KHCO_3$, no membrane, i_l=10 mA cm^{-2}, p_{CO_2} = 1 atm, boundary layer thickness = 100 µm, and $k_l a\,\delta = 0.33$ s^{-1}.

3.6 Effect of Boundary Layer Thickness

The foregoing analysis of polarization losses was conducted for boundary layers 100 µm thick, a thickness not difficult to realize in a CO2R electrochemical cell. The boundary layer thickness can be tuned by adjusting the flowrate of CO_2 and/or electrolyte. For a fixed current density or ionic fluxes, the concentrations of CO_2 and protons at cathode will decrease with increase in the boundary layer thickness (according to Fick's law). The greater is the departure of the surface concentrations from those in the bulk, the greater are the polarization losses. Figure 7

shows a monotonic increase in the polarization losses with increasing boundary layer thickness for 1M $KHCO_3$ electrolyte at 10 mA cm^{-2}. Here again, the major contributions to the polarization loss are from the cathode pH and CO_2 losses. The polarization loss at the cathode is 96% and at the anode is 4% of the total 200 mV. The solution and anode pH losses are less than 16 mV. A similar effect of boundary layer thickness on polarization losses can be expected for Figures 3b, 4a, 5, and 6. The relative magnitude of polarization losses can be affected by the boundary layer thickness, but not their rankings. To keep the polarization loss to < 200 mV requires a boundary layer thickness smaller than 188 µm. A more precise estimation of boundary layer thickness requires computational fluid dynamics simulation of a bubbly-flow in the electrochemical cell, which is outside the scope of this effort.

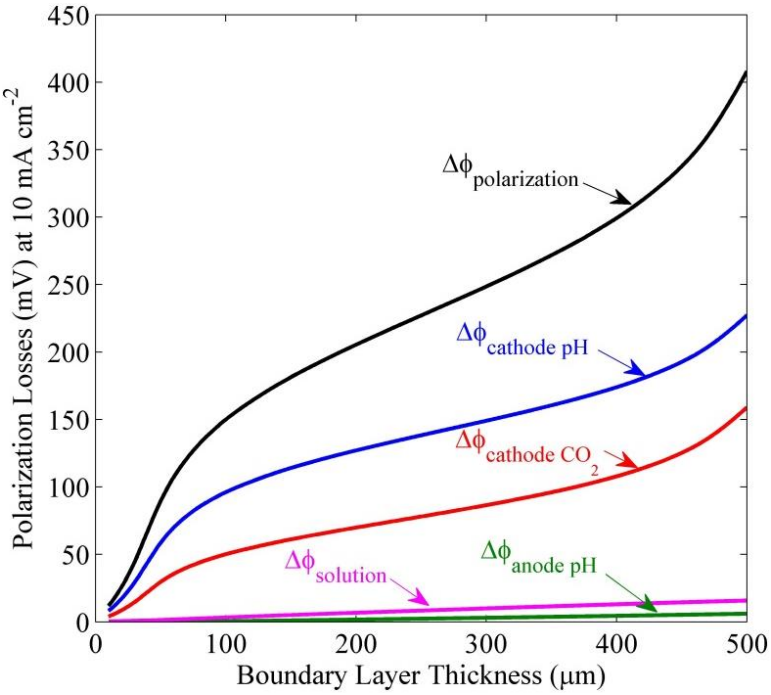

Figure 7: Increase in the polarization losses with increase in the boundary layer thickness. Operating conditions: pH 7.8, 1 M $KHCO_3$, no membrane, i_l=10 mA cm^{-2}, p_{CO_2} =1 atm, and $k_l a\,\delta = 0.33\ s^{-1}$.

3.7 Effects of Carbon Dioxide Mass-Transfer Coefficient and Partial Pressure

The electrochemical cell must be supplied with a sufficient molar flow of CO_2 to match the maximum CO_2 consumption flux of 0.52 mmol m^{-2} s^{-1} at 10 mA cm^{-2} (assuming that CO is the only product formed). The flowrate and partial pressure of CO_2 can be adjusted independently to supply the required amount of CO_2. Figure 8a shows the effect of mass-transfer coefficient of CO_2 in 1M $KHCO_3$ on the polarization losses at 10 mA cm^{-2}. The polarization losses are almost

unchanged until the mass-transfer coefficient falls below 1.67×10^{-2} s^{-1}. Thereafter, the polarization losses increase slightly with decreasing mass-transfer coefficient, resulting in subsaturated concentrations of CO_2 in the bulk. The cathode pH and CO_2 losses increase sharply for mass-transfer coefficients $<4.2\times10^{-3}$ s^{-1} because the supply rate of CO_2 is much smaller than the consumption rate, which makes the entire electrolyte alkaline. Therefore, the anode pH loss is negative. Consequently, further decrease in the mass-transfer coefficient $\left(<4\times10^{-3}\ s^{-1}\right)$ will not be possible as the current density will be mass-transfer limited. The net increase in the polarization losses caused by decreasing the mass-transfer coefficient from $1\ s^{-1}$ to 4.2×10^{-3} s^{-1} is only 41.4 mV. The corresponding changes in cathode pH loss is 25.6 mV, cathode CO_2 loss is 16.7 mV, solution loss is 1 mV, and anode pH loss is -1.9 mV.

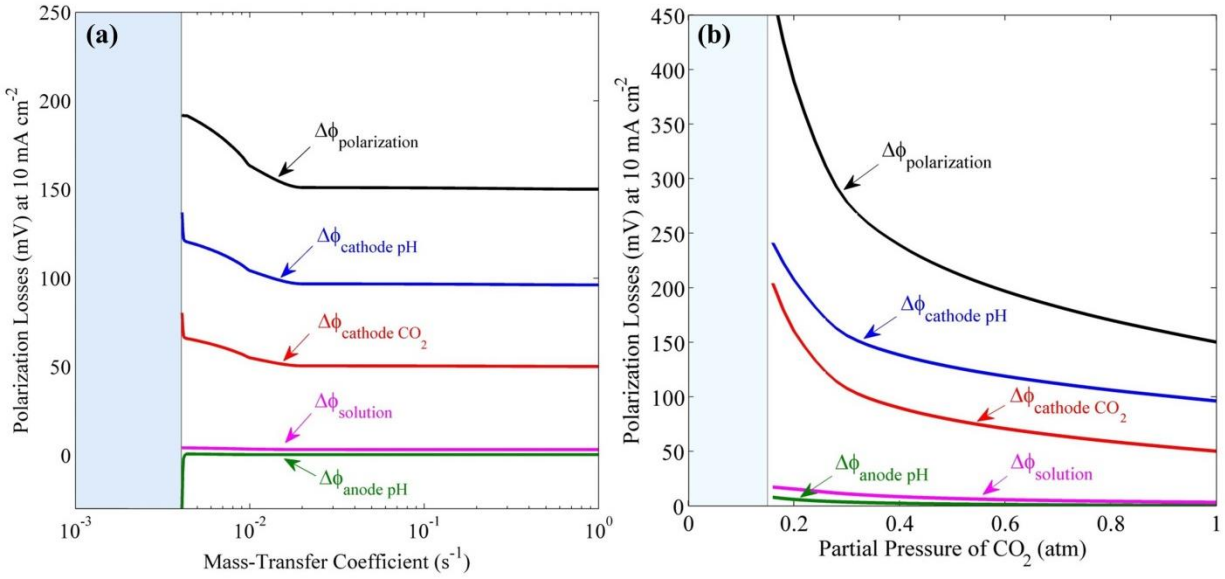

Figure 8: Variation in the polarization losses at 10 mA cm^{-2} with (a) the effective volumetric mass-transfer coefficient of CO_2 and (b) the partial pressure of CO_2. Operating conditions: (a) pH 7.8, 1 M $KHCO_3$, no membrane, i_l=10 mA cm^{-2}, p_{CO_2} =1 atm, and boundary layer thickness = 100 µm, (b) pH 7.8, no membrane, i_l=10 mA cm^{-2}, boundary layer thickness = 100 µm, and $k_l a\,\delta = 0.33\ s^{-1}$.

As mentioned above, the partial pressure of CO_2 can be adjusted for a fixed flowrate according to the consumption of CO_2 at the cathode. The operation of an electrochemical cell in an electrolyte subsaturated in CO_2 will increase the polarization of the cathode. The effects of CO_2 partial pressures in 1M $KHCO_3$ on the polarization losses are shown in Figure 8b. The polarization loss increases to ~215 mV as the partial pressure of CO_2 is reduced to 0.5 atm. Here the major sources of polarization losses are the cathode pH loss – 59%, and CO_2 loss – 37%. The

anode pH losses are less than 18 mV. The lowest partial pressure of CO_2 required to attain a current density of 10 mA cm^{-2} is 0.15 atm, which is 385 and 2 times higher than the partial pressure of CO_2 in air and flue gases, respectively. This suggests that flue gases could be a potential source of CO_2 for future CO2R electrochemical cells.

3.8 Effect of Membrane Ion Selectivity

The purpose of the membrane in an electrochemical cell is to transport the majority charge carriers and prevent the crossover of the products of CO2R. Figure 9 shows the effects of using a cation exchange membrane (CEM) versus an anion exchange membrane (AEM) on the polarization losses in 1M $KHCO_3$ electrolyte. The addition of AEM to the electrolyte causes a slight increase in the polarization loss by ~ 10 mV at 10 mA cm^{-2} over that found in the absence of a membrane. By contrast, the polarization losses produced using a CEM rise rapidly with current density, and are infinite at 10 mA cm^{-2}. The polarization losses in presence of a CEM are higher compared to those for an AEM or the absence of a membrane. Also, the limiting current density attainable using a CEM is much smaller than that attainable using an AEM. Since the majority charge carriers at steady state are carbonate and bicarbonate ions, an anion exchange membrane will be most suitable for CO2RR electrochemical cells. In the case of a CEM such as Nafion, the majority charge carriers (anions) will be blocked and potassium ions (cations) will be forced to migrate towards cathode causing electrodialysis and extremely high polarization losses. Unfortunately, most work on electrochemical CO2RR at pH 6.8 is performed with Nafion (a proton exchange membrane).

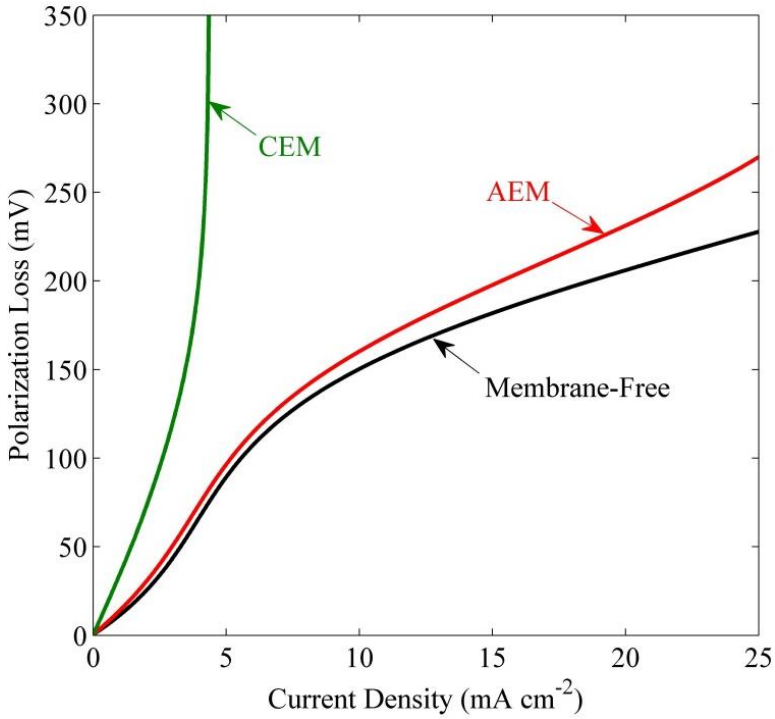

Figure 9: Comparison of polarization losses in the membrane-free 1M $KHCO_3$ electrolyte with the electrolyte separated by an anion exchange membrane (AEM) and a cation exchange membrane (CEM). Operating conditions: pH 7.8, 1 M $KHCO_3$, $p_{CO_2} = 1\,\text{atm}$, boundary layer thickness = 100 μm, and $k_l a\,\delta = 0.33\ \text{s}^{-1}$.

3.9 Effect of Catalyst Selectivity

The polarization losses will be highest for electrochemical synthesis of CO, due to high stoichiometric consumption of CO_2 per electron, as compared to other products of the CO2RRs. Figure 10 shows the current density versus cell potential and the distribution of losses for the case where an IrO_2 anode and an Ag cathode (assuming 100% CO selectivity) are used. The Butler-Volmer parameters are given in Table 2. The polarization loss is ~5.5% of the cell voltage for a current density of 10 mA cm^{-2}.

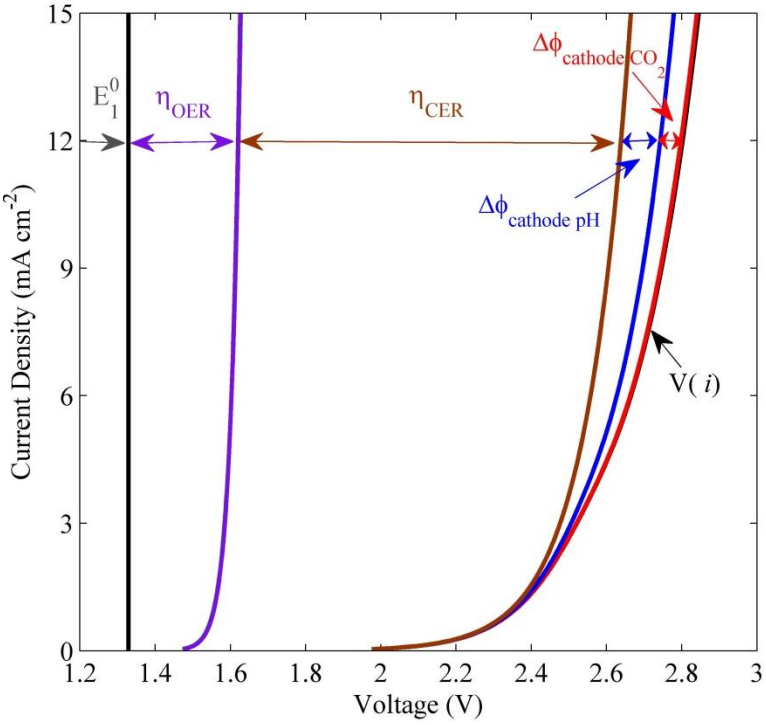

Figure 10: Current density versus applied voltage showing distribution of losses for IrO2 anode and hypothetical cathode with 100% CO selectivity. Operating conditions: pH 7.8, 1 M $KHCO_3$, no membrane, $p_{CO_2} = 1$ atm, boundary layer thickness = 100 μm, and $k_l a \delta = 0.33\ s^{-1}$. $E_1^0 = 1.33$ V is the equilibrium cell potentials for CO formation.

Figure 11a-b shows the partial current density of CO and H_2 versus cell potential and the distribution of losses for the case in which IrO_2 is used as the anode and Ag as the cathode[28]. In this case, the polarization loss decreases to ~3% of total applied potential for the current density of 10 mA cm^{-2}. Figure 11c shows the total current density as a function of cell voltage and the dependence of the faradaic efficiency of CO formation on the cell voltage. The faradaic efficiency of CO reaches a maximum value of 92.6% for an applied voltage of 2.56 V. The energy efficiency of a CO2R product is a multiplication of its faradaic efficiency and voltage efficiency, such as

$$\eta_{E,i} = \eta_{F,i}(V)\frac{\left(1.229 - E_i^0\right)}{V(i)} \qquad 23$$

where $\eta_{E,i}$ is the energy efficiency, $\eta_{F,i}$ is the faradaic efficiency, and E_i^0 is the equilibrium potential vs. RHE of i^{th} product. A plot of $\eta_{E,i}$ versus applied voltage is given in Figure 11d, which shows that $\eta_{E,i}$ reaches a maximum value of 49.1% at an applied voltage of 2.47 V.

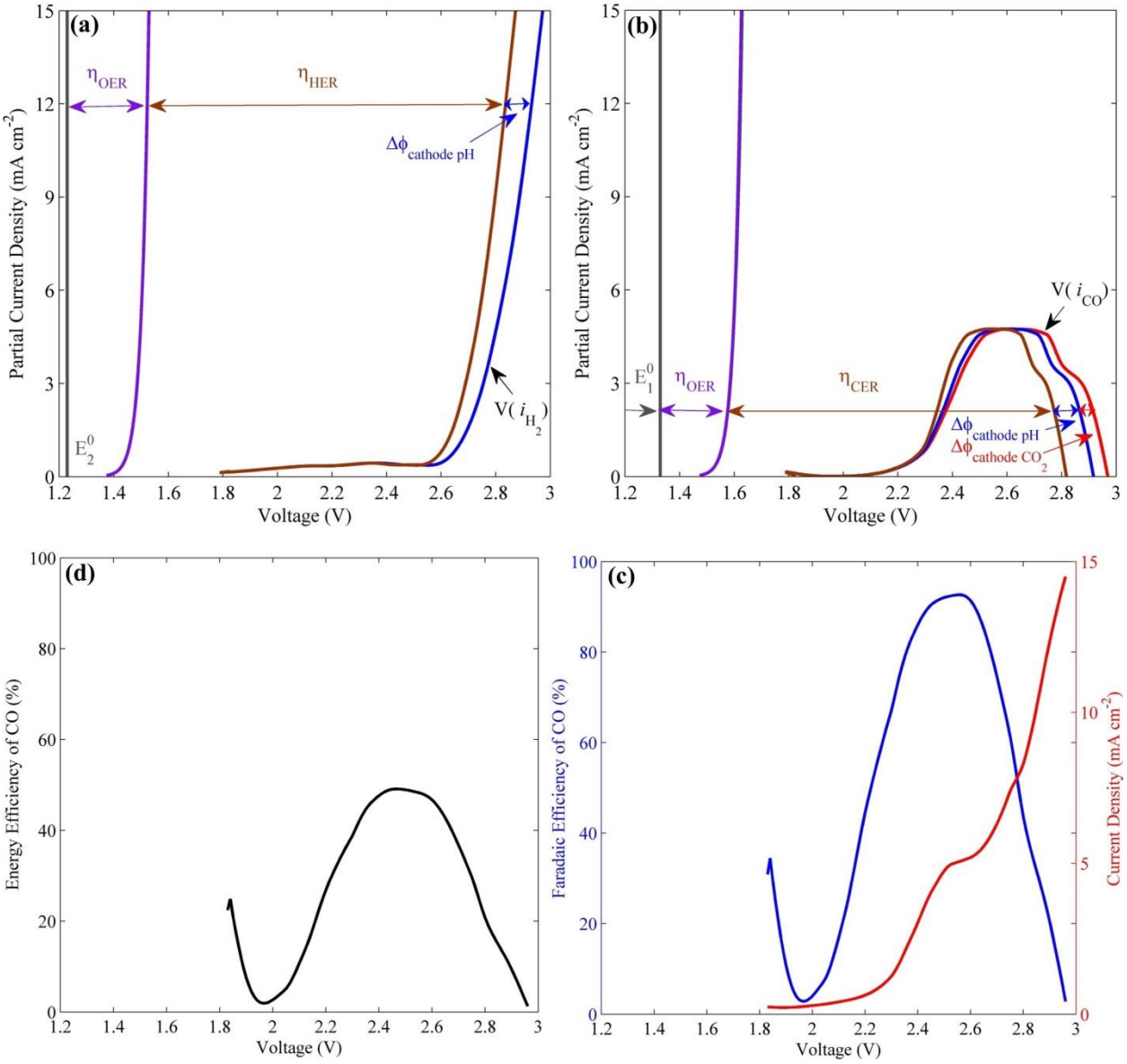

Figure 11: a-b) Partial current density versus cell potential showing the distribution of losses for CO and H_2 formation on Ag, (c) Total current density and faradaic efficiency of CO formation, (d) Energy efficiency of CO formation. Operating conditions: pH 7.8, 1 M $KHCO_3$, no membrane, $p_{CO_2} = 1$ atm, boundary layer thickness = 100 µm, and $k_l a \delta = 0.33\ s^{-1}$. $E_1^0 = 1.33$ V and $E_2^0 = 1.23$ V are the equilibrium cell potentials for CO and H_2 formation, respectively.

It should be noted that the polarization losses decrease as the number of moles of CO_2 consumed per transferred electron decreases. This trend occurs because the decrease in the consumption of CO_2 per electron-transferred decreases the depletion of CO_2 at the cathode, which in turn reduces the polarization losses. In general, the polarization losses for various CO2RR products obey the following trend:

$$CH_4 < C_2H_4 = C_2H_5OH = CH_3OH < HCOO^- = CO$$

It is possible to obtain enhanced catalytic activity using photo-generated carriers, which can further reduce kinetic overpotentials for CO_2 reduction.[31] However, the polarization losses will remain the same for solar-enhanced catalytic reactions, as it is only dependent on the photocurrent density, operating conditions, and chemical composition of electrolyte and membrane.

3.10 Effect of Polarization Losses on Catalyst Activity Measurements

The electrode polarization is inevitable in any electrochemical cell as the current density passed through the cell approaches the limiting current density. Figure 12 shows the observed partial current densities versus the cathode potential (vs RHE) for six major products reported by Kuhl et al.[2] Also shown are with the calculated values of the pH and CO_2 concentration at the cathode. The polarization is not significant up to -1 V vs RHE. However, below an applied voltage of -1.1 V vs RHE which correspond to a total current density of > 8 mA cm^{-2}, the CO_2 concentration decreases rapidly to 0.1 mM and the pH rises to 9.5. The effects of polarization losses on the kinetic overpotentials of individual products of the CO2RR are presented in the supplementary information. The behavior of Tafel plots below -1 V vs RHE is due to polarization of the electrode and does not represent the intrinsic activity of copper at pH 6.8.

The preceding illustration demonstrates that there are two principal consequences of excessive polarization on electrocatalytic measurements: The first is the increase in pH near the cathode, which causes a decrease in the local CO_2 concentrations and, consequently both the pH and the CO_2 concentration deviate significantly from their corresponding values in the bulk electrolyte. Second, as the applied potential rises, the fraction of the total potential available to drive the CO2RR decreases. This is what causes the kinetic overpotential to become smaller as the applied potential is further increased, a pattern that is seen in Figures S1a-b. A further consequence of high Nernstian overpotentials is the increase in the selectivity to H_2 generation relative to the products of CO2R, a trend that has been reported for H_2 evolution.[32] This conclusion is also supported by recent measurements, which show that the kinetic overpotentials for the HER occurring on NiMo and NiFe are lower under alkaline than under acidic conditions.[33] The decrease in the partial current densities of ethylene and ethanol seen in Figure 12 are actually due to a decrease in the kinetic overpotentials, as shown in Figure S1b. This observation supports the finding of Hori et al.[34] that the kinetics of ethylene evolution is pH independent. The cause for the observed decrease in the overpotential of methane evolution at higher current densities (or higher pH) is due to decrease in the partial current densities of C2 products. Schouten et al. also found that the increase in the partial current density of methane is coupled with higher hydrogen production in the alkaline electrolyte.[32] Therefore, the change in the faradaic efficiency of CO2RR products for cathode voltages below -1V vs RHE is due to the increase in the pH at the cathode and is not a characteristic property of copper at pH 6.8.

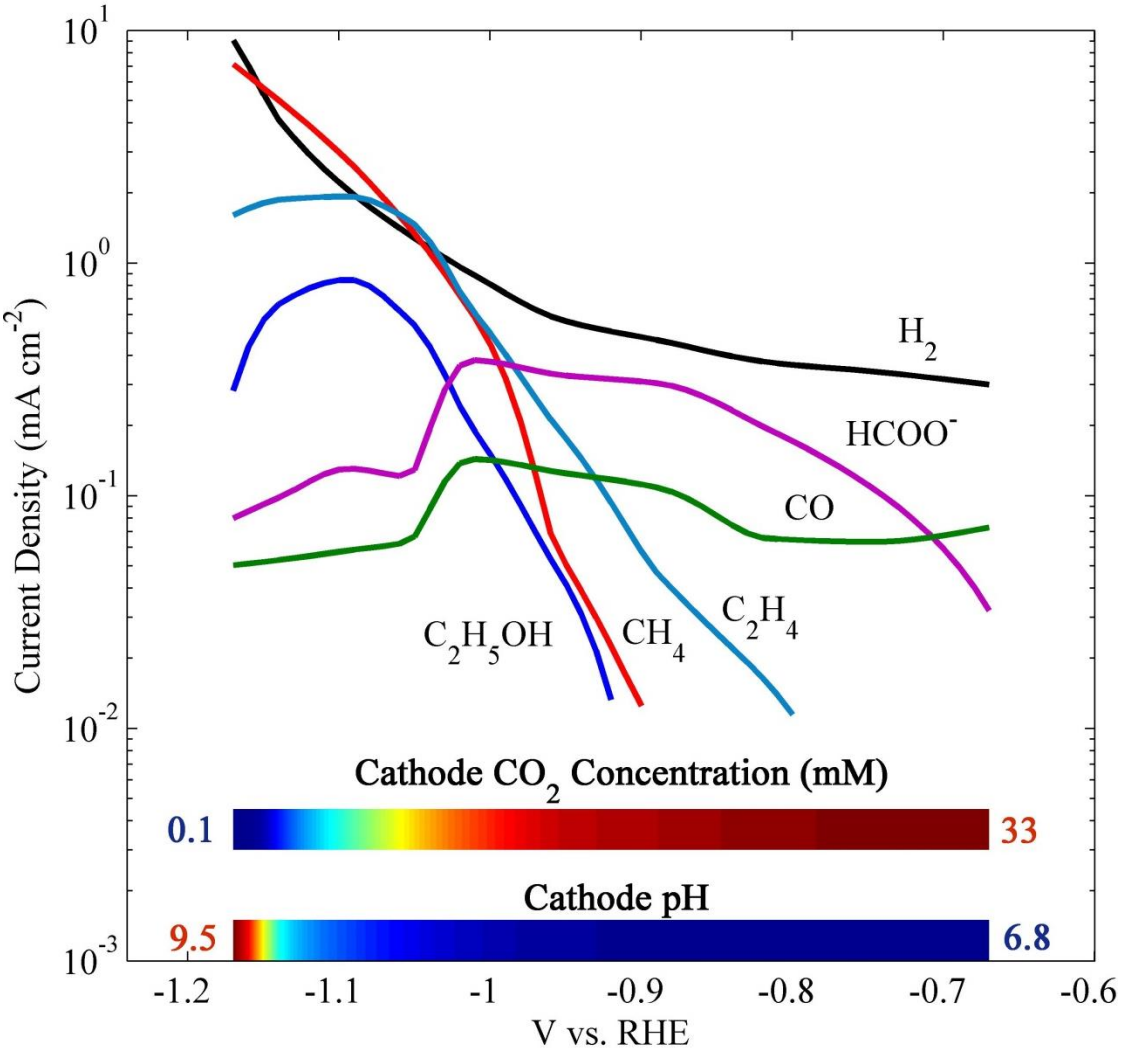

Figure 12: Measured partial current density versus applied voltage for six major products as reported by Kuhl et al.[2], and calculated surface pH and CO_2 concentration versus applied voltage. Operating conditions: pH 6.8, 0.1M $KHCO_3$, 100 µm Selemion AMV (AEM), $p_{CO_2} = 1$ atm, electrode spacing = 3.56 cm, boundary layer thickness = 40 µm, $k_l a \delta = 0.042$ s^{-1} (corresponding to a flowrate of 20 cm^3 min^{-1}).

4. CONCLUSIONS

This study has shown that the electrochemical reduction of CO_2 is affected by many factors. These include the composition of the catalysts used for the OER and CO2RR, the pH and conductivity of the electrolyte, the composition of the membrane separating the anolyte from the catholyte, and the voltage applied across the cell. We find that the bulk pH of the electrolyte strongly affects polarization losses occurring at the electrodes and, in turn, the limiting current density at which the cell can be operated. To achieve high limiting current densities and conditions favoring the reduction of CO_2 versus the generation of H_2, the electrolyte should be

close to neutral in pH. The addition of a pH buffer lowers polarization losses for a given cell current density but may suppress the selectivity to products of the CO2RR.[30] Polarization losses are also reduced by using an anion- rather than a cation-exchange membrane and by reducing the mass-transfer boundary layer near each electrode. For a given current density, the highest level of polarization occurs for CO2RR catalysts exhibiting a high selectivity to CO, and the level of polarization decreases as the number of electrons required to produce a molecule of product increases. All other factors being constant, the level of electrode polarization increases with increasing current density. Therefore, the proposed analysis of polarization losses can also be used to study CO2R PECs[35] operating at current density of < 1 mA cm^{-2} (see Figure 4a).

The results of this study suggest that reported measurements[2] of the electrochemical reduction of CO_2 are strongly affected by polarization losses at higher current densities (> 5 mA cm^{-2}). As demonstrated in Figures 12 and Figure S1, high polarization losses are due to the increase in pH at the cathode surface, which leads to a reduction in the local concentration of CO_2 and a reduction in the kinetic overpotential. Consequently, the changes in product currents and Faradaic efficiencies reported at high applied potentials and correspondingly high total current densities should not be interpreted as intrinsic characteristics of the CO2R catalyst, since such results are strongly affected by cathode polarization. This finding leads to the recommendation that electrochemical studies of the CO2RR be conducted in a manner that avoids conditions under which strong cathode polarization occurs. One approach for doing so would be to monitor the pH near the cathode surface. A technique for doing so based on measurement of the open circuit voltage at the cathode has been described in the literature.[36] Alternatively, the methods described here can be used to predict the limiting current and operating conditions to avoid exceeding 80% of the limiting current. We note further that significant depletion of CO_2 from the electrolyte can lead to an increase in polarization losses, as can poor mass transfer to the cathode. Therefore, electrochemical cells used for studies of the CO2RR should be designed to have high rates of gas to liquid mass transfer and thin mass-transfer boundary layers. These conditions can be achieved by supplying the cell with a high flow rate of electrolyte saturated with CO_2 and by maintaining a small inter-electrode gap.

5. ACKNOWLEDGEMENTS

This material is based on the work performed by the Joint Center for Artificial Photosynthesis, a DOE Energy Innovation Hub, supported through the Office of Science of the U.S. Department of Energy under Award number DE-SC0004993. We are grateful to Prof. John S. Newman for his valuable suggestions and comments. We also thank Kendra Kuhl and Toru Hatsukade for providing experimental data for CO_2 reduction on copper and silver electrodes.

REFERENCES

1. Y. Hori, in *Modern aspects of electrochemistry*, Springer, 2008, pp. 89-189.
2. K. P. Kuhl, E. R. Cave, D. N. Abram and T. F. Jaramillo, *Energy & Environmental Science*, 2012, **5**, 7050-7059.
3. I. C. Man, H. Y. Su, F. Calle-Vallejo, H. A. Hansen, J. I. Martínez, N. G. Inoglu, J. Kitchin, T. F. Jaramillo, J. K. Nørskov and J. Rossmeisl, *ChemCatChem*, 2011, **3**, 1159-1165.
4. C. C. McCrory, S. Jung, J. C. Peters and T. F. Jaramillo, *Journal of the American Chemical Society*, 2013, **135**, 16977-16987.
5. M. Gattrell, N. Gupta and A. Co, *Journal of Electroanalytical Chemistry*, 2006, **594**, 1-19.
6. J. Jin, K. Walczak, M. R. Singh, C. Karp, N. Lewis and C. Xiang, *Energy & Environmental Science*, 2014.
7. M. R. Singh, J. C. Stevens and A. Z. Weber, *Journal of The Electrochemical Society*, 2014, **161**, E3283-E3296.
8. D. Friebel, M. W. Louie, M. Bajdich, K. E. Sanwald, Y. Cai, A. M. Wise, M.-J. Cheng, D. Sokaras, T.-C. Weng and R. Alonso-Mori, *Journal of the American Chemical Society*, 2015.
9. W. Li, *ChemInform*, 2012, **43**, no.
10. K. P. Kuhl, T. Hatsukade, E. R. Cave, D. N. Abram, J. Kibsgaard and T. F. Jaramillo, *Journal of the American Chemical Society*, 2014, **136**, 14107-14113.
11. N. Gupta, M. Gattrell and B. MacDougall, *Journal of applied electrochemistry*, 2006, **36**, 161-172.
12. C. Delacourt and J. Newman, *Journal of The Electrochemical Society*, 2010, **157**, B1911-B1926.
13. C. Delacourt, P. L. Ridgway and J. Newman, *Journal of The Electrochemical Society*, 2010, **157**, B1902-B1910.
14. U. Riebesell, V. J. Fabry, L. Hansson and J.-P. Gattuso, *Guide to best practices for ocean acidification research and data reporting*, Publications Office of the European Union Luxembourg, 2010.
15. A. L. Soli and R. H. Byrne, *Marine Chemistry*, 2002, **78**, 65-73.
16. K. G. Schulz, U. Riebesell, B. Rost, S. Thoms and R. Zeebe, *Marine chemistry*, 2006, **100**, 53-65.
17. P. Atkins and J. De Paula, *Atkins' physical chemistry*, Oxford University Press, 2014.
18. J. Newman and K. E. Thomas-Alyea, *Electrochemical systems*, John Wiley & Sons, 2012.
19. M. Flury and T. F. Gimmi, *Methods of Soil Analysis: Part 4 Physical Methods*, 2002, 1323-1351.
20. B. Jähne, G. Heinz and W. Dietrich, *Journal of Geophysical Research: Oceans (1978–2012)*, 1987, **92**, 10767-10776.
21. R. E. Treybal and E. Treybal Robert, *Mass-transfer operations*, McGraw-Hill New York, 1968.
22. L. Labík, R. Vostal, T. Moucha, F. Rejl and M. Kordač, *Chemical Engineering Journal*, 2014, **240**, 55-61.

23. P. Wilt, *Journal of Colloid and Interface Science*, 1986, **112**, 530-538.
24. Z. Samec, A. Trojanek and E. Samcova, *The Journal of Physical Chemistry*, 1994, **98**, 6352-6358.
25. A. Herrera and H. Yeager, *Journal of The Electrochemical Society*, 1987, **134**, 2446-2451.
26. K.-L. Huang, T. M. Holsen and J. R. Selman, *Industrial & engineering chemistry research*, 2003, **42**, 3620-3625.
27. A. M. Kiss, T. D. Myles, K. N. Grew, A. A. Peracchio, G. J. Nelson and W. K. Chiu, *Journal of The Electrochemical Society*, 2013, **160**, F994-F999.
28. T. Hatsukade, K. P. Kuhl, E. R. Cave, D. N. Abram and T. F. Jaramillo, *Physical Chemistry Chemical Physics*, 2014, **16**, 13814-13819.
29. M. R. Singh, E. L. Clark and A. T. Bell, *Manuscript Under Preparation*, 2015.
30. Y. Hori, A. Murata, R. Takahashi and S. Suzuki, *Journal of the Chemical Society, Chemical Communications*, 1988, 17-19.
31. B. Kumar, M. Llorente, J. Froehlich, T. Dang, A. Sathrum and C. P. Kubiak, *Annual review of physical chemistry*, 2012, **63**, 541-569.
32. K. J. P. Schouten, Z. Qin, E. P. r. Gallent and M. T. Koper, *Journal of the American Chemical Society*, 2012, **134**, 9864-9867.
33. C. C. McCrory, S. Jung, I. M. Ferrer, S. Chatman, J. C. Peters and T. F. Jaramillo, *Journal of the American Chemical Society*, 2015.
34. Y. Hori, R. Takahashi, Y. Yoshinami and A. Murata, *The Journal of Physical Chemistry B*, 1997, **101**, 7075-7081.
35. T. Sekimoto, S. Shinagawa, Y. Uetake, K. Noda, M. Deguchi, S. Yotsuhashi and K. Ohkawa, *Applied Physics Letters*, 2015, **106**, 073902.
36. S. Hessami and C. W. Tobias, *AIChE journal*, 1993, **39**, 149-162.